An X-ray Backlit Talbot-Lau Deflectometer for High-Energy-Density electron density diagnostics

M. P. Valdivia[1], D. Stutman[1], C. Stoeckl[2], W. Theobald[2], C. Mileham[2], I. Begishev[2], J. Bromage[2], S. P. Regan[2]

[1] Department of Physics and Astronomy, Johns Hopkins University, Baltimore, MD 21218
[2] Laboratory for Laser Energetics, U. of Rochester, Rochester, NY 14623

X-ray phase-contrast techniques can measure electron density gradients in high-energy-density plasmas through refraction induced phase shifts. An 8 keV Talbot-Lau interferometer consisting of free standing ultrathin gratings was deployed at an ultra-short, high-intensity laser system using K-shell emission from a 1-30 J, 8 ps laser pulse focused on thin Cu foil targets. Grating survival was demonstrated for 30 J, 8 ps laser pulses. The first x-ray deflectometry images obtained under laser backlighting showed up to 25% image contrast and thus enabled detection of electron areal density gradients with a maximum value of $8.1 \pm 0.5 \times 10^{23}$ cm^{-3} in a low-Z millimeter sized sample. An electron density profile was obtained from refraction measurements with an error of <8%. The 50 ± 15 μm spatial resolution achieved across the full field of view was found to be limited by the x-ray source-size, similar to conventional radiography.

I. INTRODUCTION

The Talbot-Lau interferometer is a phase-contrast diagnostic used in medical and biological applications **[1, 2]** recently adapted for use in High Energy Density (HED) plasma experiments **[3, 4, 5]**. The Talbot-Lau X-ray Deflectometry (TXD) technique can deliver electron density gradients from x-ray refraction angle measurements and provide additional simultaneous information such as attenuation **[4]**, elemental composition (Z_{eff}) mapping **[5]**, and small-angle scatter **[6]**. TXD is a powerful low-Z matter diagnostic for x-ray energies in the range of 10-100 keV because the refraction signature is much stronger than attenuation in this energy range.

Refraction can be a powerful HED diagnostic, particularly for Inertial Confinement Fusion (ICF) experiments since implosion capsules are mostly composed of low-Z materials **[7]**, and hence, it can present advantages over standard attenuation based plasma density diagnostics. Recently, it has been shown that TXD provides diagnostic capabilities beyond electron density measurements **[8]**. TXD can simultaneously diagnose refraction and attenuation, and by combining these two, it can diagnose material mixing through elemental composition measurements. The diagnostic can also detect the presence of micro-instabilities through small-angle scatter measurements **[6]**.

The TXD technique has been benchmarked in the laboratory using x-ray tubes (copper, tungsten, and molybdenum anode) as sources, where its performance as an electron density diagnostic in a HED relevant geometry was first tested **[3, 4, 5]**. In order to investigate the capabilities of the Talbot-Lau interferometer as an electron density diagnostic in a HED plasma experiment, the feasibility of the TXD technique in such an environment must be validated. Such an experiment should demonstrate Talbot pattern formation and electron density retrieval using a high power laser-target interaction to produce an x-ray backlighter as a viable x-ray source. Therefore, a test under laser produced x-ray illumination was performed on the Multi-TeraWatt (MTW) facility at the Laboratory for Laser Energetics (LLE) **[9, 10, 11, 12]**. The MTW laser is a single-beam, hybrid chirped-pulse amplification laser system used as a prototype front-end test bed for the OMEGA-EP laser facility **[13, 14]** and as backlighter development platform.

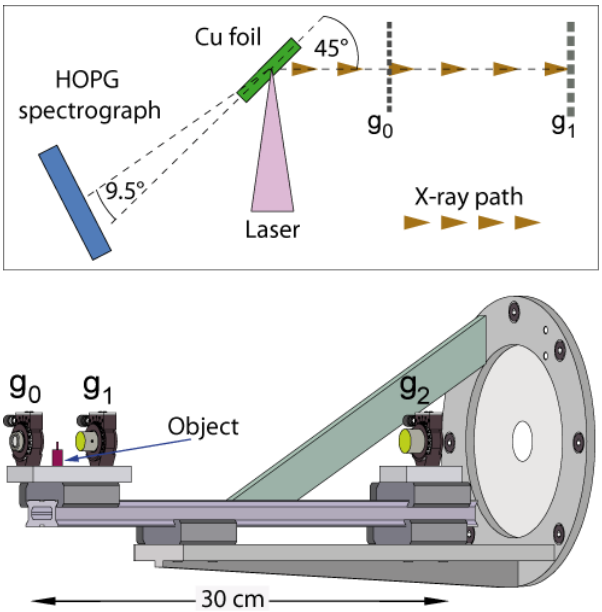

Figure 1. Above: X-ray backlighter illumination schematic in reference to the source and phase gratings (g_0 and g_1) and the spectrograph view angle. Below: Interferometer rail system deployed at MTW. The Talbot-Lau interferometer setup is similar to the interferometer presented in Ref. {**4**}

II. TALBOT-LAU INTERFEROMETER SETUP

The Talbot-Lau (TL) interferometer, shown in **Figure 1**, was mounted on an 8 inch port cover in the MTW target chamber. The TL interferometer was composed of a source grating (g_0) of 2.4 µm period, a phase grating (g_1) of 4.0 µm period, and an analyzer grating (g_2) of 12 µm period. In order to transmit 8 keV x-rays, the gold and nickel gratings are membrane supported **[4]**. The objects to be imaged, either an acrylic rod or a flouro-nylon fiber, were placed between g_0 and g_1. The source grating was located anywhere between 9 and 35 mm from the laser foil target, which is placed at the center of the MTW chamber. The interferometer orientation was such that it viewed the copper target 45° off the target normal.

The Moiré deflectometry images were recorded using an Andor Ikon-M x-ray CCD camera, which was mounted behind the analyzer grating g_2, along the TL interferometer and target line of sight. The camera has an array of 1024×1024 pixels of 13 µm. The CCD chip was cooled to –65°C to reduce dark current. The camera detector plane was located ~500 mm from the laser target, giving the Talbot-Lau interferometer system an overall object magnification of ~9. The x-ray emission from the copper K-lines was measured through x-ray spectroscopy using a Highly Oriented Pyrolytic Graphite (HOPG) crystal spectrometer [**15**].

In TXD, the dynamic range of the electron density measurement depends on the x-ray energy, Talbot geometry/grating period dimensions, and object to grating distance. Additionally, the system spatial resolution will also limit the electron density retrieving capabilities in the Fourier filtering process. The Talbot order used **[1,2]** was determined by the object to grating distance restriction imposed by MTW target chamber geometry and the angular sensitivity required to appropriately retrieve electron density information from the objects probed with the Cu x-ray backlighter. More details on geometrical characteristics and restrictions are further detailed in Ref {**3,4**}. The distance between source and phase gratings was 44 mm. The object was located 31 mm from the source grating, hence the effective angular resolution was W_{eff} ~77 µrad. In general, the lower limit for fringe shift measurements is ~1%, which translates to ± 0.8 µrad refraction angle for the TL setup used. The fringe shift measurement upper limit is one period, which is well above the fringe shift observed in the experimental images. It should be noted that better system angular and spatial

resolutions would yield higher fringe shifts, particularly at the rod edges, which will be explored in future experiments.

III. X-RAY BACKLIGHTER

The MTW laser delivered a 1.054 μm beam of 1-30 J in 8 ps, to a Cu foil of 500 × 500 μm^2 area and 20 μm thickness with on-target intensities of 10^{17}-10^{19} W/cm^2. The Talbot-Lau Interferometer viewed the target at an angle of 45°. About 50% of the laser energy was focused onto a 5 μm diameter spot using an f/2.5 off-axis parabola at a 45° angle of incidence, as shown in **Figure 1**. The laser-plasma interactions generated target confined energetic electrons giving way to copper K-shell emission; K_α at 8.05 keV and K_β at 8.91 keV, originating from the cold bulk material during the fast electron lifetime **[16, 17]**. The laser was defocused up to 134 μm on the target surface in order to reduce the hard x-ray background.

The backlighter radiation was filtered by a combination of thin foils. A protective filter, either 50 μm aluminized Mylar or 25 μm aluminum, was set in front of the source grating and an additional filter of 25 μm copper or 25 μm aluminum was placed in front of the x-ray CCD in order to prevent stray light from reaching the detector. The combination of foils filtered out x-rays below 4 keV, so that the radiation transmitted through the interferometer consisted primarily of 8-9 keV copper K-shell x-rays. **Figure 2** shows K_α and K_β emission curve for the copper anode x-ray tube source, the theoretical interferometer fringe contrast curve ($Contrast = \frac{I_{max}-I_{min}}{I_{max}+I_{min}}$, where I_{max} and I_{min} are the maximum and minimum fringe intensity, respectively), and the transmission curves for the filter foils. The expected interferometer contrast curve was computed with the XWFP code [**18**] using the grating parameters and including the geometrical broadening of the Talbot pattern by the finite source grating openings. The selected filters allowed for interferometer contrast of 30% using a copper anode x-ray tube as source and 27% at MTW with the copper x-ray backlighter source.

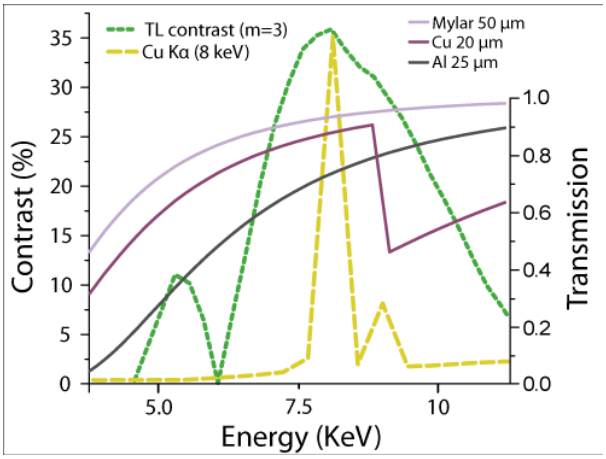

Figure 2. Left axis: Interferometer contrast curve. Right axis: Filter transmission curves. Copper anode x-ray tube emission (a.u.) shown as well.

III. EXPERIMENTAL RESULTS

In order to assess the TXD performance under laser driven x-ray backlighter illumination, a variety of parameters were studied. Backlighter x-ray output and source size delivered important information about spectral quality and spatial resolution. Source grating survival was tested at target-to-grating distances of ~1 to 4 cm and laser energies between 1-30 J. Lastly, photon count and interferometer contrast were evaluated in order to determine if

the x-ray backlighter output and the resulting Moiré image allowed accurate electron density retrieval.

A. Backlighter spectrum

Previous studies **[18]** analyzed K_α backlighter emission where a peak of 70 μm spatial half-width was found to be surrounded by a 400 μm diameter halo of weak K_α emission corresponding to two-thirds of the K_α emission. Additionally, the K_α intensity at the source center did not increase with increasing laser intensity and the size of the halo increased when the laser intensity was increased. These findings indicate that the large x-ray backlighter source size obtained (~80 μm FWHM) could be due to a distribution of x-rays within a range of intensities and/or energies. Furthermore, it was observed that the emission spectrum contains a continuum background extending to higher x-ray energies, which could affect the overall spot size of the backlighter.

Figure 3 shows the copper backlighter spectra recorded with the HOPG spectrometer obtained for a 30 J, 8 ps laser pulse defocused at 134 μm. The conversion efficiency calculated using the HOPG spectrograph data was found to be 3 x 10^{-5}, with a 0.30 K_β/K_α ratio. This value is unusually high, particularly when compared to the ratio of 1.15 obtained in **Ref {21}**. The high K_β/K_α ratio measured could be a result of the significant radiation re-absorption in the direction of the HOPG spectrometer due to the very shallow angle of view onto the foil (9.5 degrees with respect to the foil surface, as shown in **Figure 1**), so that the opacity correction model used in these calculations might not be the most accurate match. Therefore, since the optical thickness for the K_α line was higher than the optical thickness for the K_β line in the plasma, it lead to a higher detected ratio for this particular configuration. It should also be noted that any alignment errors in the detector angle of view will have a large effect on the measured HOPG signal, which might explain the relatively high shot to shot fluctuation that was observed as well. Furthermore, the laser was defocused in order to optimize contrast by reducing the hard x-ray background component from the backlighter emission while the pulse duration was stretched from 1 ps to 8 ps. Laser defocusing results in a much lower laser intensity, which correlates with a lower K_α signal. Previous studies have shown that the conversion efficiency of laser energy into K_α signal decreases with laser intensity below ~1x10^{18} W/cm^2 **[21]**.

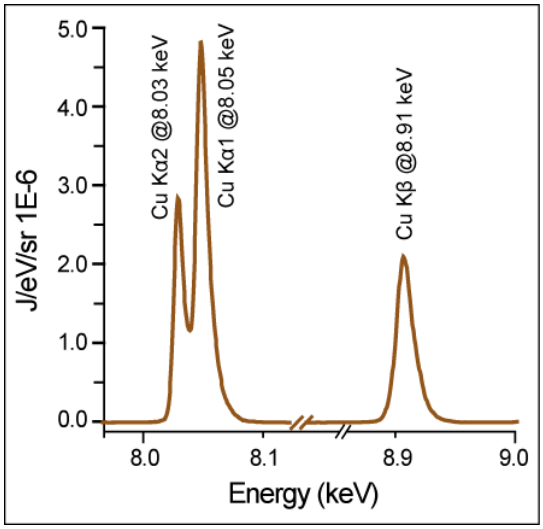

Figure 3. Cu K_α and Cu K_β emission spectrum recorded with the HOPG spectrometer for 30 J, 8 ps laser shots defocused by 134 μm.

A more systematic and thorough investigation of backlighter source size, where K-line emission size can be measured independently from higher energy source size, could be performed using a curved crystal imager **[22]**. Additionally, backlighter spectra should be characterized beyond source size and K-line emission in follow-up experiments to properly evaluate the optimal backlighter characteristics needed for TXD diagnostics. Moreover, the hard x-ray background from the direct line of sight between the source and the detector could be reduced by filtering the x-ray source with reflective optics. This new configuration would limit the backlighter emission to the 8 keV range, which could potentially deliver a smaller source size from pure Cu K-edge emission. Given that higher energies would not be a concern for this particular setup, laser de focusing would not be necessary, hence the overall intensity would increase, positively impacting the photon statistics with the potential added benefit of a smaller source size.

B. Source grating survival

Because low-energy Talbot-Lau gratings are free standing membranes, grating survival assessment was one of the main tasks in the experiment. The high x-ray radiation produced by the laser-target interaction can potentially ablate the source grating bars and/or cause them to expand, thus affecting the Talbot pattern. The source grating is the most vulnerable to the laser-target interaction given its proximity to the foil target and small period. The g_0 grating is made of 2.4 μm period gold bars with a maximum tolerable expansion of ~0.1 μm (<5% of the period). The grating disassembly time is given by the plasma sound speed (C_s) and if we assume a charge state Z~10 for gold, then C_s[μm/ps] ~0.0036 $T^{1/2}$ [eV]. Thus, an expansion of 0.1 μm in 10 ps would require a temperature of ~5.3 eV.

At a few millimeters from the backlighter, g_0 is far enough to not be directly heated by the laser backlighter. Based on Ref. **{23}**, only a small fraction of relativistic electrons would reach the grating from the backlighter foil. Therefore, the backlighter emission of soft x-rays is expected to be the main heating mechanism. Considering a laser backlighter of 100 J with 30% soft x-ray conversion efficiency 3 mm away from the source grating, then the x-ray fluence is ~0.3 J/mm^2 at the grating location. If 100% of the soft x-ray are absorbed in the gold bars and assuming all the absorbed energy goes into increasing the gold temperature, the estimation of T ~1 eV indicates that any morphological variation in grating geometry would occur after the main x-ray pulse originated from the picosecond backlighter. These calculations suggest that the interferometer should be able to deliver an accurate Moiré deflectometry image before any morphological changes occur in the gratings.

The first TXD measurements using a laser driven x-ray backlighter at MTW experimentally demonstrated grating survival for laser energies of up to 30 J, and pulse duration of 8 ps. The protective foil placed directly in front of the source grating kept it from direct interaction with the x-ray backlighter even at a grating to target distance of ~1 cm. Nevertheless, grating survival and accurate Moiré image retrieval should be explored for smaller distances and using higher power lasers which would serve as scaling and reference point for future grating survival studies.

Phase grating survival and further testing of source grating survival will be the focus of future experiments. Consequently, an OMEGA EP experiment would allow performing TXD under typical HED experimental conditions with a plasma object, where not only can the source grating be modified by the backlighter x-rays, but the phase grating can be also be affected by plasma heating and emission. It should be noted that grating survival is only necessary for the duration of Moiré pattern acquisition. Therefore, if gratings are modified once the acquisition has taken place, they can be replaced shot-to-shot, at a reasonable cost.

C. Photon count

For a single laser pulse of 30 J, 8 ps, the x-ray CCD recorded, on average, approximately 15,000 counts per pixel. This translates to 12 photons absorbed and, taking into account the 40% quantum efficiency, the number of photons incident per pixel is ~30. The photon count, although low, was found to be adequate for image processing, and while there is room for further improvement by increasing laser intensity, we were able to obtain fringe shift information from the Moiré images and the respective angular refraction maps were retrieved with a 50 ± 15 µm spatial resolution. Note, however, that increasing laser intensity will in turn impact grating survivability.

D. Spatial resolution

A Moiré image obtained for a 1 mm diameter acrylic rod at MTW is shown in **Figure 4**. Using the edge method we obtained an x-ray backlighter FWHM of ~75 ± 12 µm. Furthermore, the experimental Moiré image was compared to simulations **[19]** in order to determine source size. As observed in the figure, a FWHM of ~80 µm was found to be the best match, agreeing with the direct source size edge measurement. These comparison images demonstrate that smaller source sizes will deliver better refraction angle characterization, specially at interfaces, which is highly relevant when measuring material mixing.

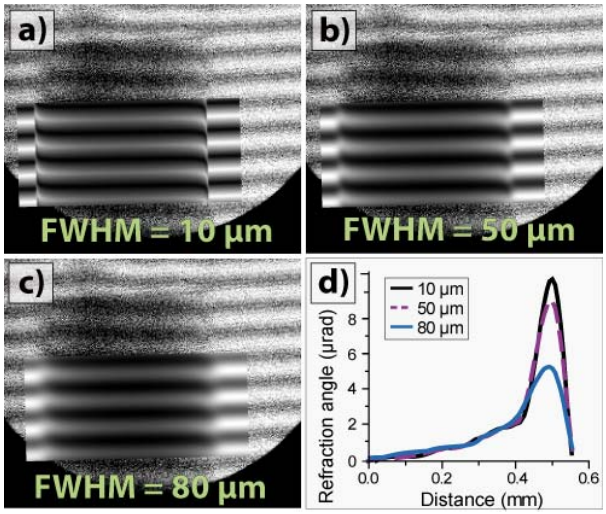

Figure 4. Experimental Moiré image of a 1 mm diameter acrylic rod obtained at MTW using an 8 keV copper K-line backlighter. For comparison, simulated Moiré patterns are superposed for sources of a) 10 µm, b) 50 µm, and c) 80 µm FWHM. Additionally, a plot with the refraction angle profiles for these three simulated sources is shown in (d).

E. Interferometer contrast

Fringe contrast is an important parameter in Talbot interferometry. Phase retrieval codes rely on accurate fringe shift tracking, therefore better contrast improves the electron density gradient retrieval process. In the laboratory we achieved a maximum contrast of 30% using an x-ray copper anode tube, while under x-ray backlighter illumination at MTW we obtained a maximum of 27%. This result is quite encouraging, in particular when considering the low photon statistics in the MTW configuration explored.

When evaluating phase retrieval accuracy, it must be considered that variations (errors) in the phase retrieval maps are almost exclusively due to both photon count and experimental interferometer contrast, as shown in Ref. {**24**}. It should also be considered that the experimental interferometer contrast is also dependent on the noise level present in the imaging system. Moreover, the contrast to noise ratio in phase images (obtained through

refraction techniques) is higher when compared to attenuation images. Additionally, given that the noise vs. resolution trade-off is less efficient for phase imaging, phase contrast imaging performs best for high resolution systems, which is encouraging for HEDP applications where high spatial resolution is required **[25]**. Moreover, the noise level issue can be improved with better photon statistics and imaging detector, analogous to other diagnostics.

As seen in **Figure 2**, the x-ray backlighter spectrum is relevant when considering TXD performance improvement through interferometer contrast. Emission of copper K_α and K_β for laser pulses of 1-10 J, 1-10 ps has been demonstrated in previous publications **[26, 27]**. Similarly, for higher energies (300-2100 J), the backlighter spectrum also contains He_α and Ly_α lines generated from hot surface plasma **[28, 29]**. Since the contrast curve for our interferometer in the third Talbot order **[30]** has a peak at 8.0 keV, with a FWHM of 3.4 keV, any combination of the aforementioned copper emission lines would produce high interferometer contrast, as observed experimentally. Interferometer setups for low Talbot orders (e.g., m=1) would deliver higher contrast while orders up to m=7 **[4]** would deliver interferometer contrast of about 25%. These numbers are encouraging for configurations using the present laser parameters as well as for higher power lasers, which is the next step in benchmarking the TXD technique as a HED diagnostic.

F. Electron density measurement

A Moiré image of an acrylic rod of 750 μm diameter and a fluoro-nylon fiber of 305 μm diameter, obtained using the TXD diagnostic at MTW with an x-ray backlighter, is shown in **Figure 5**. The interferometry image (**Fig 5b**) shows the profile of both objects, easily distinguishable by their respective x-ray attenuation signatures, where the thicker plastic rod (left) is more attenuating than the thinner fluoro-nylon fiber (right). The fringe pattern obtained in the presence of these objects is shifted due to x-ray refraction induced by the line integrated areal electron density gradient. Since the x-ray refraction angle is proportional to the fringe shift, a refraction angle map can be retrieved from the measured fringe shifts between the object and reference images [**3, 4, 5**]. A line profile of x-ray refraction angle, averaged over one period, is shown in **Figure 5c** for each of the objects.

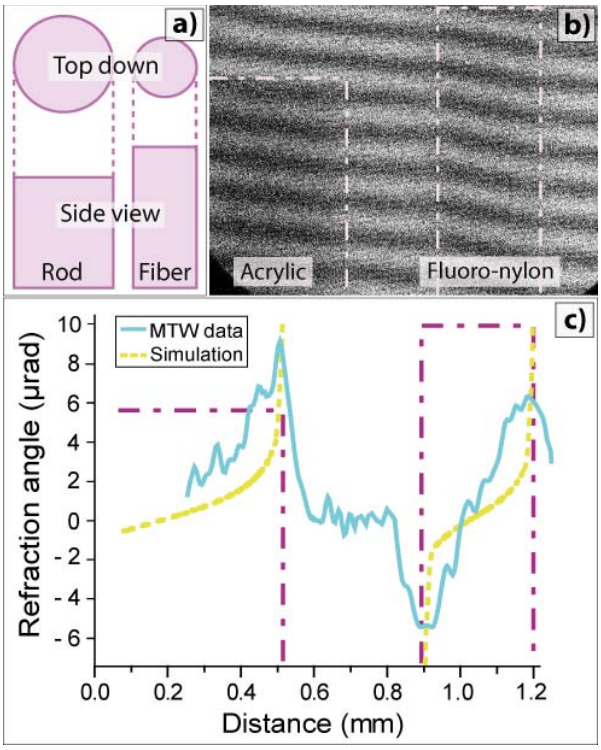

Figure 5. a) Top down and side view diagrams of the samples imaged. b) Experimental Moiré images of an acrylic rod of 750 mm diameter and a fluoro-nylon fiber of 305 µm diameter (outlined with a semi-dashed line). c) Plot of the one period averaged line profiles for the simulated (dotted line) and the experimentally retrieved (solid line) refraction angle.

TXD phase retrieval methods **[3]** were applied to obtain a fringe shift map, which was scaled in order to retrieve the fluoro-nylon fiber and the acrylic rod refraction angle profiles. The maximum angular refraction measured for the fluoro-nylon was ~6 µrads and ~9 µrads for the 0.75 mm diameter acrylic rod.

Previous TXD laboratory measurements showed a peak refraction angle of ~21 µrad at the edge of a 0.75 mm diameter acrylic rod. These measurements used an anode x-ray tube of 15 µm source FWHM. The difference in maximum refraction angle measured is mainly due to the smaller spatial resolution achieved with the copper x-ray tube when compared to the copper target laser backlighter (10 µm v/s 50 µm). Nonetheless, this can be attributed to a blurring artifact which is not a problem special to TXD, since similar results would be expected from propagation images. Overall, the MTW refraction measurements are accurate but, due to the large source size and hence low spatial resolution, they are a poorer match to the theoretical refraction profiles, in particular near object edges.

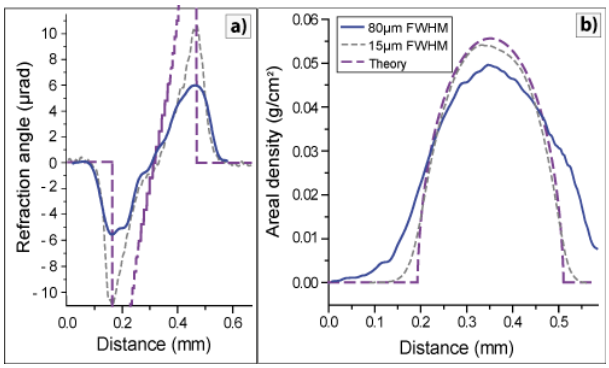

Figure 6. Theoretical and experimental (a) areal electron density and (b) x-ray refraction angle profiles for the 305 μm diameter fluoro-nylon fiber. Experimental results are shown for a copper anode x-ray tube (15 μm FWHM) and for the MTW experiment using a copper K-line backlighter (~80 μm FWHM), along with simulated results.

A similar comparison of laboratory and MTW results can be made for the fluoro-nylon object. **Figure 6a** shows an additional angle of refraction profile obtained at MTW for the fluoro-nylon fiber along with the profiles obtained in a laboratory setting using a copper x-ray tube and a theoretical refraction profile. Horizontal numerical integration and scaling of the x-ray refraction angle map (**Fig 6a**) delivered an areal electron density map (**Fig 6b**). These plots indicate that source size is a highly relevant parameter when performing TXD measurements since it directly impacts spatial resolution, and thus, it has a strong effect in electron density retrieval. If Gaussian blurring is taken into account, the overall areal electron density profiles are accurate. This is also evident in the simulated profiles shown in **Figure 4**.

However, in addition to the statistical noise, the edges of the areal electron density profile can deviate from the expected values (as seen in **Fig. 6b**) due to iterative centering methods not being included in the trapezoidal numerical integration of refraction angle profiles. Much information has been reported elsewhere about proper integration of peak functions and the comparison between integration methods **[31]**. Moreover, the application of better integration methods in Moiré image processing would improve the overall electron density retrieval accuracy. In particular, given that axial symmetry is expected in most of the HEDP experiments which would benefit from Talbot-Lau interferometry, Abel inversion methods should be further explored. Furthermore, generalized Abel inversion for non axi-symmetric objects should be analyzed and developed as well **[32]** in order to obtain a comprehensive density retrieval method for the TXD technique.

An areal electron density value of 0.050 ± 0.001 g/cm^2 was obtained at the center of the fluoro-nylon fiber when probed with the x-ray backlighter at MTW. Using the sample symmetry information, a local electron density value of 1.66 ± 0.03 g/cm^3 was retrieved. Given that the tabulated density value for this particular fluoro-nylon sample is not available, the results were compared to the tabulated values of 1.78 g/cm^3 for Polyvinylidene Fluoride, thus yielding an error of <8%. In contrast, an error of <6% was found through the TXD method using a laboratory source of 15 μm FWHM.

The underestimation of electron density and areal electron density values is expected considering our sources of error in measurement and calculations in addition the small dimensions of the probed object (when compared to the probing source size). Nonetheless, the results detailed above are encouraging, particularly considering the large backlighter source size. The comparison with simulated profiles and tabulated values demonstrates that TXD could be a reliable and accurate electron density diagnostic for HED plasmas. However, further studies under improved experimental conditions are needed to benchmark the TXD technique. Namely, the results here shown indicate that source size backlighter quality improvement should deliver even more accurate electron density information.

SUMMARY:

The Talbot-Lau X-ray Deflectrometry technique has been demonstrated using laser backlighter x-ray illumination. We tested its capabilities as an HED diagnostic for electron density mapping. Grating survival was demonstrated with 30 J, 8 ps laser pulses 1 cm away from the target. High contrast images were obtained even at low photon count with a system spatial resolution of ~50 μm. The Moiré images obtained at MTW with an 8 keV x-ray backlighter show fringe shifts of under 10% with an angular sensitivity of 80 μrads. Considering that the TXD technique is capable of obtaining fringe shifts of a few periods, the given electron density range for the diagnostic is ~$2\text{x}10^{23}$ to ~$2\text{x}10^{25}$ cm^{-3}. The results

obtained suggest the TXD technique in combination with high power laser backlighter systems would provide a better photon budget and thus, should yield Moiré images capable of delivering electron density information in HED plasma experiments, in particular for ICF applications, with an error of <8%.

It should be noted that the imaging limitations here observed (such as spatial resolution and statistical noise) impact the TXD technique in the same way that radiography diagnostics would be affected. Therefore, the limitations are not unique to the TXD technique, but rather a common blurring artifact due to the x-ray backlighter characteristics. In brief, the overall imaging conditions can and should be optimized through backlighter improvement. Even considering these limitations, the preliminary results here presented show the potential capabilities of TXD as a viable diagnostic for HED plasma experiments.

ACKNOWLEDGMENTS:

This work is supported by U.S. DoE/NNSA Grant No. DENA0001835.

REFERENCES:

[1] F. Pfeiffer, T.Weitkamp, O.Bunk, and C. David, Nature Physics 2, 258 (2006)
[2] A. Momose, W. Yashiro, Y. Takeda, Y. Suzuki and T. Hattori, Japanese Journal of Applied Physics Vol. 45, 5254 (2006)
[3] M. P. Valdivia, D. Stutman, and M. Finkenthal, Journal of Applied Physics 114, 163302 (2013)
[4] M. P. Valdivia, D. Stutman, and M. Finkenthal, Review of Scientific Instruments 85, 073702 (2014)
[5] M. P. Valdivia, D. Stutman, and M. Finkenthal, Applied Optics 54, 2577 (2014)
[6] L. Hackermüller, K. Hornberger, B. Brezger, A. Zeilinger, and M. Arndt, Applied Physics B 77, 8 781-787 (2003)
[7] J. Lindl, O. Landen, J. Edwards, E. Moses, NIC Team, Phys. Plasmas 21, 020501 (2014)
[8] M. P. Valdivia, D. Stutman, and M. Finkenthal, " A Talbot-Lau X-Ray Deflectometer as a High Energy Density Plasma Diagnostic", submitted to special issue of the IEEE journal Transactions on Plasma Science, IEEE Symposium on Fusion Engineering (2015)
[9] V. Bagnoud, I. Begishev, M. J. Guardalben, J. Puth, and J. D. Zuegel, in Proceedings of Conference on Lasers and Electro-Optics/International Quantum Electronics Conference and Photonic Applications Systems Technologies, Optical Society of America, San Francisco, CA, 2004, paper JTuE4.
[10] V. Bagnoud, I. A. Begishev, M. J. Guardalben, J. Puth, and J. D. Zuegel, Opt. Lett. 30, 1843 (2005).
[11] V. Bagnoud, J. Puth, I. Begishev, M. Guardalben, J. D. Zuegel, N. Forget, C. L. Blanc, and J. Bromage, in Proceedings of Conference on Lasers and Electro-Optics/Quantum Electronics and Laser Science and Photonic Applications Systems Technologies, Optical Society of America, Baltimore, MD, 2005, paper JFA1,
[12] C. Dorrer, I. A. Begishev, A. V. Okishev, and J. D. Zuegel, Opt. Lett. 32, 2143 (2007)
[13] L. Waxer, T. K. D.N. Maywar, J. H. Kelly, R. M. B.E. Kruschwitz, S. J. Loucks, C. S. D. D. Meyerhofer, S. F. B. Morse, and J. Zuegel, Opt. Photonics News 16, 30 (2005)
[14] C. Stoeckl, S.-W. Bahk, J. Bromage, V. Y. Glebov, O. V. Gotchev, P. A. Jaanimagi, D. D. Meyerhofer, P. Nilson, T. C. Sangster, M. Storm, S. Sublett, W. Theobald, and J. D. Zuegel, paper presented at 9th International Fast Ignition Workshop, Cambridge, MA
[**15**] W. Theobald, V. Ovchinnikov, S. Ivancic, B. Eichman, P. M. Nilson, J. A. Delettrez, R. Yan , G. Li, F. J. Marshall, D. D. Meyerhofer, J. F. Myatt, C. Ren, T. C. Sangster, C. Stoeckl, J. D. Zuegel, L. Van Woerkom, R. R. Freeman, K. U. Akli, E. Giraldez and R. B. Stephens, Physics of Plasmas (1994-present) 17, no. 10 (2010): 103101.
[16] J. Myatt, Theobald, W., Delettrez, J. A., Stoeckl, C., Storm, M., Sangster, T. C., Maximov, A. V., and Short, R. W., Phys. Plasmas 14(5), 056301 (2007).
[17] Nilson, P. M., Theobald, W., Myatt, J., Stoeckl, C., Storm, M., Gotchev, O. V., Zuegel, J. D., Betti, R., Meyerhofer, D. D., and Sangster, T. C., Phys. Plasmas 15(5), 056308 (2008).
[18] T. Weitkamp, C. David, C. Kottler, O. Bunk, and F. Pfeiffer. "Tomography with grating interferometers at low-brilliance sources." In SPIE Optics+ Photonics, pp. 63180S-63180S. International Society for Optics and Photonics, 2006.
[19] T. Weitkamp, Advances in Computational Methods for X-Ray and Neutron Optics, edited by Manuel Sanchez del Rio, Proc. of SPIE Vol. 5536, pp. 181-189. 2004
[20] C. Reich, I. Uschmann, F. Ewald, S. Düsterer, A. Lübcke, H. Schwoerer, R. Sauerbrey, E. Förster, and P. Gibbon, Physical Review E 68, no. 5 (2003): 056408.

[21] P. M. Nilson, W. Theobald, J. F. Myatt, C. Stoeckl, M. Storm, J. D. Zuegel, R. Betti, D. D. Meyerhofer, and T. C. Sangster, Physical Review E 79, no. 1 (2009): 016406.
[22] C. Stoeckl, G. Fiksel, D. Guy, C. Mileham, P. M. Nilson, T. C. Sangster, M. J. Shoup III, and W. Theobald, Review of Scientific Instruments 83, no. 3 (2012): 033107.
[23] E. E. Fill. Physics Of Plasmas, 12(5):052704, 2005
[24] T. Weber, P. Bartl, F. Bayer, J. Durst, W. Haas, T. Michel, A. Ritter, and G. Anton, Medical physics 38, no. 7 (2011): 4133-4140.
[25] T. Köhler, K. J. Engel, and E. Roessl, Medical physics38, no. S1 (2011): S106-S116.
[26] P. M. Nilson, W. Theobald, J. F. Myatt, C. Stoeckl, M. Storm, J. D. Zuegel, R. Betti, D. D. Meyerhofer, T. C. Sangster, Physical Review E 79, no. 1 (2009): 016406.
[27] P. M. Nilson, A. A. Solodov, J. F. Myatt, W. Theobald, P. A. Jaanimagi, L. Gao, C. Stoeckl R. S. Craxton,2 J. A. Delettrez, B. Yaakobi, J. D. Zuegel, B. E. Kruschwitz, C. Dorrer, J. H. Kelly, K. U. Akli, P. K. Patel, A. J. Mackinnon, R. Betti, T. C. Sangster, D. D. Meyerhofer, Physics of Plasmas 18, no. 5 (2011): 056703.
[28] P. M. Nilson, A. A. Solodov, J. F. Myatt, W. Theobald, P. A. Jaanimagi, L. Gao, C. Stoeckl, R. S. Craxton, J. A. Delettrez, B. Yaakobi, J. D. Zuegel, B. E. Kruschwitz, C. Dorrer, J. H. Kelly, K. U. Akli, P. K. Patel, A. J. Mackinnon, R. Betti, T. C. Sangster, and D. D. Meyerhofer, Physical review letters 105, no. 23 (2010): 235001.
[29] W. Theobald, K. Akli, R. Clarke, J. A. Delettrez, R. R. Freeman, S. Glenzer, J. Green, G. Gregori, R. Heathcote, N. Izumi, J. A. King, J. A. Koch, J. Kuba, K. Lancaster, A. J. MacKinnon, M. Key, C. Mileham, J. Myatt, D. Neely, P. A. Norreys, H.-S. Park, J. Pasley, P. Patel, S. P. Regan, H. Sawada, R. Shepherd, R. Snavely, R. B. Stephens, C. Stoeckl, M. Storm, B. Zhang, and T. C. Sangster, Physics of Plasmas (1994-present) 13, no. 4 (2006): 043102.
[30] M. Engelhardt, C. Kottler, O. Bunk, C. David, C. Schroer, Joachim Baumann, M. Schuster, and F. Pfeiffer, Journal of microscopy 232, no. 1 (2008): 145-157.
[31] K. Ohta and H. Ishida, Applied Spectroscopy 42, no. 6 (1988): 952-957.
[32] P. Tomassini and A. Giulietti, Optics Communications 199, no. 1 (2001): 143-148.